Amin Soltani, An Deng, Abbas Taheri, Mehdi Mirzababaei & Mark B. Jaksa

A dimensional description of the unconfined compressive strength of artificially cemented fine-grained soils

Journal of Adhesion Science and Technology, 2020; 34(15):1679-1703

A Dimensional Description of the Unconfined Compressive Strength of Artificially-Cemented Fine-Grained Soils

Amin Soltani [1,*], An Deng [2], Abbas Taheri [3], Mehdi Mirzababaei [4] and Mark B. Jaksa [5]

[1] **Research Fellow** — Department of Infrastructure Engineering, Melbourne School of Engineering, The University of Melbourne, Parkville, VIC 3010, Australia; Amin.Soltani@unimelb.edu.au; ORCID

[2] **Senior Lecturer** — School of Civil, Environmental and Mining Engineering, The University of Adelaide, Adelaide, SA 5005, Australia; An.Deng@adelaide.edu.au; ORCID

[3] **Senior Lecturer**; School of Civil, Environmental and Mining Engineering, The University of Adelaide, Adelaide, SA 5005, Australia; Abbas.Taheri@adelaide.edu.au; ORCID

[4] **Senior Lecturer** — School of Engineering and Technology, Central Queensland University, Melbourne, VIC 3000, Australia; M.Mirzababaei@cqu.edu.au; ORCID

[5] **Professor** — School of Civil, Environmental and Mining Engineering, The University of Adelaide, Adelaide, SA 5005, Australia; Mark.Jaksa@adelaide.edu.au; ORCID

* **Correspondence:** Amin Soltani; Amin.Soltani@unimelb.edu.au; ORCID

Abstract: This study aims at establishing a universal predictive model for the unconfined compressive strength (UCS) of artificially-cemented fine-grained soils. Model development, its validation and calibration were carried out using a comprehensive database gathered from the research literature. The dimensional analysis concept was successfully extended to the soil–cement UCS problem, thereby leading to a practical dimensional model capable of simulating the UCS as a function of the blend's index properties — that is, cement content, specific surface area, curing time, and the compaction state parameters (including water content and dry density). The predictive capability of the proposed model was examined and further validated using routine statistical tests, as well as conventional fit-measure indices which resulted in $R^2 > 0.95$ and NRMSE < 5%. A sensitivity analysis was also carried out to quantify the relative impacts of cement content, curing time and soil plasticity on the UCS. The higher the soil plasticity, the higher the positive sensitivity to cement content, implying that soils of higher plasticity would require higher cement contents for stabilization. On the contrary, the higher the soil plasticity, the lower the positive sensitivity to curing time, indicating a more effective cement hydration in soils of lower plasticity. Finally, an explicit calibration procedure, involving a total of three UCS measurements for three recommended soil–cement mix designs, was proposed and validated, thus allowing for the proposed model to be implemented with confidence for predictive purposes, preliminary design assessments and/or soil–cement optimization studies.

Keywords: Soil–cement; Unconfined compressive strength; Dimensional analysis; Cement content; Curing time; Specific surface area; Compaction state; Sensitivity analysis

Abbreviations: AI: Artificial intelligence; ANN: Artificial neural network; CAH: Calcium–Aluminate–Hydrates; CASH: Calcium–Aluminate–Silicate–Hydrates; CSH: Calcium–Silicate–Hydrates; DDL: Diffused double layer; GP: Genetic programing; MLR: Multiple linear regression; NRMSE: Normalized root-mean-squared error; PSO: Particle swarm optimization; RMSE: Root-mean-squared error; UCS: Unconfined compressive strength; USCS: Unified Soil Classification System

1. Introduction

Fine-grained soils, particularly those of medium–high plasticity, are the most common and readily accessible of all materials encountered in construction operations [1]. Such soils, however, are often characterized as inferior/problematic construction materials, as their intrinsic mechanical attributes — such as high compressibility, low shear strength, and high moisture susceptibility —

present significant challenges for road construction, building foundations, earth dams and other geotechnical engineering systems [2,3]. These adverse behaviors are often amended by means of soil stabilization techniques. The term "stabilization" refers to any physical, chemical or combined physical–chemical practice of altering the soil fabric to satisfy the intended mechanical/design criteria [4]. Physical stabilization practices often include soil replacement, pre-wetting, compaction and/or reinforcement [5]. The latter, reinforcement, involves the placement of randomly-distributed or systematically-engineered geosynthetics — such as fibers, geogrids, geocomposites and geocells — in the soil regime, thus interlocking the soil particles into a unitary mass of improved mechanical performance [6–12]. Chemical stabilization refers to the addition of chemical agents — mainly cementitious binders such as Portland cement and lime, and more recently polymers, resins and sulfonated oils — to the soil–water medium, thereby encouraging particle flocculation (and/or aggregation) and hence the development of a dense, uniform matrix coupled with enhanced mechanical properties [13–19].

Soil–cement can be defined as a blend of pulverized soil, Portland cement and water, which is often compacted to a high density, e.g., standard or modified Proctor optimum condition, and achieves a hard, semi-rigid fabric over time. Despite some environmental concerns, the use of Portland cement still remains the most well-established and time-tested soil stabilization scheme practiced over the past century, owing to its excellent resistance against weathering and mechanical forces [4,14]. The governing variables which influence/control the mechanical performance of soil–cement have been well documented in the research literature. However, the time-consuming nature of soil–cement testing suggests the need for a more practical alternative to adequately perceive and hence predict its short- and long-term mechanical performance, particularly in terms of shear strength. Such a predictive framework, if developed, would aid the geotechnical engineer in arriving at optimum soil–cement design choices without the hurdles of conducting time-consuming laboratory tests. More importantly, in view of cement's high energy consumption and carbon footprint, the ability to identify/predict the optimum soil–cement mix design for a desired application can lead to significant cost and environmental benefits. In this context, a number of studies have proposed various forms of empirical/regression, physical and constitutive models capable of simulating the shear strength, mainly unconfined compressive strength (UCS), of compacted soil–cement blends [20–27]. In addition, the use of artificial intelligence (AI) techniques — including artificial neural networks (ANNs), genetic programing (GP), and metaheuristic optimization algorithms such as particle swarm optimization (PSO) — have also shown great promise in describing and hence simulating the UCS of compacted soil–cement blends [28–31]. The majority of these models, however, suffer from limited predictive capability and/or time-consuming and often sophisticated calibration procedures. The so-called "limited predictive capability" refers to the models being restricted to certain soil types, specific curing times (mainly seven days) and/or particular cement types and contents. In essence, the available models are mainly impractical and hence may not be trivial to implement in practice [32]. Accordingly, the development of an objective model, capable of addressing the aforementioned limitations, is required.

Quite clearly, the development of a universal predictive model accounting for all variables governing a physical problem, in this case the UCS of soil–cement, is a formidable task. The dimensional analysis concept, also recognized as Buckingham's Pi theorem, offers a feasible path towards incorporating and hence unifying a large number of input variables into a simple physical model capable of adequately describing a desired output variable [33]. Despite the concept's successful adoption as a fundamental principle in fluid mechanics, its application has been less extended to geotechnical-related problems, particularly for stabilized soil systems including soil–cement blends [34–36]. Accordingly, this study aims at establishing a universal predictive model, by means of the dimensional analysis concept, for the UCS of artificially-cemented fine-grained soils. Model development, its validation and calibration were carried out by means of a comprehensive soil–cement database gathered from the research literature. A sensitivity analysis was also carried out to quantify the relative impacts of the model's input variables, namely cement content, curing time and soil plasticity, on the UCS. Finally, a practical calibration framework was proposed and validated, thus allowing for the proposed dimensional model to be implemented with confidence for predictive purposes, preliminary design assessments and/or soil–cement optimization studies.

2. Soil–Cement Database

A comprehensive database of 171 UCS tests was gathered from the research literature, and was used to extend the dimensional analysis concept to the soil–cement UCS problem. The compiled database consisted of fifteen fine-grained soils — hereafter referred to as datasets and denoted as S_n where $n = \{1, 2, \ldots, 15\}$ — of varying geological and mineralogical origins, gradations and plasticity features, each tested for UCS at varying binder (or cement) contents (i.e., binder-to-soil mass ratio) and curing times [37–47]. For each dataset, the natural soil (no binder) and various soil–cement blends were tested for UCS at their respective standard or modified Proctor optimum condition. A detailed description of the natural soils' grain-size distribution, plasticity characteristics and corresponding classification — obtained in accordance with the Unified Soil Classification System (USCS) [48] — is presented in Table A1 of the Appendix A section. Figure 1 illustrates the location of the fifteen natural soil samples, i.e., S_1 to S_{15}, on Casagrande's plasticity chart. As demonstrated in the figure, the assembled database covers a wide range of possible plasticity characteristics encountered by natural fine-grained soils, and thus provides a reliable basis for the development (and validation) of a universal soil–cement UCS model. Relevant details with regards to the implemented testing scheme for each dataset — including the selected compaction/molding states, and the binder properties (e.g., type of cement, its content and specific surface area) — are summarized in Table A2 of the Appendix A section. Finally, the variations of the reported UCS data against curing time for the fifteen soil–cement datasets, i.e., S_1 to S_{15}, are provided in Figure A1 (see Appendix A).

3. Dimensional Analysis of Soil–Cement

3.1. Governing Variables and Model Development

In the presence of water, calcium-based binders such as Portland cement initiate a series of primary and secondary chemical reactions in the soil–water medium, which amend the soil fabric into a coherent matrix of enhanced strength performance. The primary reactions consist of cement hydration and cation exchange. The former involves the hydration of calcium silicates and calcium aluminates, both major components of cement, with water, thereby resulting in the formation and propagation of strong cementation products/gels — that is, calcium–silicate–hydrates (CSH) and calcium–aluminate–hydrates (CAH) — which contribute towards the development of a uniform, dense matrix and hence an improved shear strength [14,49]. In general, cement hydration takes place almost independently of the nature of the host soil [49]. The cation exchange process, which occurs only in the presence of negatively-charged clay minerals, involves higher-valence cations substituting those of lower valence, and cations of larger ionic radius replacing those of the same valence with a smaller ionic radius [1,4,50,51]. In general, the order of cation substitution follows the Hofmeister (or lyotropic) series — that is, $Ca^{2+} > Mg^{2+} >> K^+ > Na^+$ [52]. The cementitious binder supplies the clay–water complex with excessive calcium cations (Ca^{2+}), which immediately replace cations of lower valence (e.g., sodium Na^+) and/or same-valence cations of smaller ionic radius (e.g., magnesium Mg^{2+}) on the surfaces of the negatively-charged clay particles. These cation exchanges lead to a decrease in the thickness of the diffused double layers (DDLs), attributed to the formation of strong van der Waals bonds between adjacent clay particles in the matrix, thereby resulting in flocculation of the clay particles coupled with enhanced early-age strength and improved soil workability [14,53]. A by-product of the cement hydration stage is calcium hydroxide or $Ca(OH)_2$, which produces secondary reactions with any pozzolan material present in the host soil [14,49]. Pozzolanic reactions are strongly time- and often temperature-dependent. During pozzolanic reactions, ionized calcium (Ca^{2+}) and hydroxide (OH^-) units, both released from $Ca(OH)_2$, gradually react with silica (SiO_2) and alumina (Al_2O_3) units in the host soil, thereby producing additional CSH, CAH, and possibly CASH, products in the matrix. These new cementation products encourage further flocculation and solidification of the soil particles, and thus lead to a further improvement in the soil's shear strength [5,54]. It should be noted that the commencement and evolution of the soil–cement amending reactions, which govern the development of strength in an artificially-cemented soil, are dependent on the adopted soil–binder mix design and its intrinsic physical attributes — that is, cement type and its content, curing duration, specific surface area, and the blend's compaction/molding state parameters, namely water content, dry density (or void ratio) and matric suction [23].

A practical dimensional model can be characterized as one that maintains a perfect balance between simplicity, i.e., ease of application, and accuracy, i.e., high goodness-of-fit and low forecast error [36]. These criteria imply that any proposed dimensional model should warrant a reliable prediction of the physical problem at hand while involving a minimal number of readily-measurable physical parameters (as input variables) linked together by means of a simple functional expression containing a limited number of model/fitting coefficients. Accordingly, it is essential to avoid the introduction of any input variable which is equally or more difficult to measure compared with the physical problem intended to be modeled; in some cases, an infeasible input variable can be replaced by a more-conventional (and readily-measurable) alternative [55]. For instance, it is well accepted that the mechanical performance of an unsaturated geomaterial, in this case the UCS of compacted soil–cement, is a function of the composite's as-compacted/molding hydration state and hence is governed by its matric suction. However, an accurate measurement of matric suction, particularly for fine-grained and artificially-cemented soils, requires implementing time-consuming and often sophisticated laboratory procedures [56,57]. Meanwhile, the UCS test, the problem at hand, is deemed as a routine test commonly performed in most laboratories with much less effort. As such, to maintain model practicality, matric suction should be either disregarded as an input variable or replaced by a feasible alternative, such as water content or degree of saturation. It should be noted that this simplification is in agreement with most of the existing literature, where various forms of empirical and dimensional models have been developed and validated for a variety of geomaterials without allocating matric suction as an input variable [32,36,58–62].

Taking into account the aforementioned criteria for model practicality, as well as the outlined discussions on soil–water–cement interactions, the governing input variables with respect to the soil–cement UCS problem can be categorized as: (**i**) mass of soil solids m_S; (**ii**) mass of cementitious binder m_B; (**iii**) mass of water m_W; (**iv**) initial or as-compacted dry density of the mixture composite ρ_d^M; (**v**) initial specific surface area of the mixture S_a^M; (**vi**) curing time T_c; and (**vii**) net total minor principal stress σ_3^*. Therefore, the soil–cement UCS problem can be represented by the following generic expression (all variables are in SI units):

$$\sigma_1^* = f(m_S, m_B, m_W, \rho_d{}^M, S_a{}^M, T_c, \sigma_3^*) \tag{1}$$

where f = an unknown multivariable functional expression; and σ_1^* = net total major principal stress.

For unconfined compression testing conditions, the net major and net minor total principal stresses can be, respectively, expressed as [32]:

$$\sigma_1^* = \sigma_o + \sigma_1 = q_u \tag{2}$$

$$\sigma_3^* = \sigma_o + \sigma_3 = \sigma_o \tag{3}$$

where σ_1 = total major principal stress; σ_o = atmospheric pressure (= 101,325 Pa); q_u = UCS; and σ_3 = total minor principal stress (= 0 for unconfined compression testing conditions).

The Buckingham Pi theorem states that any physical system involving N number of physical parameters with M number of basic physical dimensions/units — that is, length [L], mass [M], time [T], temperature [θ], electric current [I], amount of substance [N] and luminous intensity [J] — can be simplified to a new system involving $K = N - M$ number of dimensionless variables capable of adequately describing the original system at hand [33]. The original soil–cement UCS problem given in Equation (1) can be characterized as a system of $N = 7$ physical parameters (ρ_d^M is related to m_S and m_B and hence is not enumerated) with $M = 3$ basic physical dimensions, namely length [L], mass [M] and time [T]. Accordingly, it can be simplified to a new system involving the following $K = 7 - 3 = 4$ dimensionless variables:

$$D_o = \frac{\sigma_1^*}{\sigma_3^*} = \frac{q_u}{\sigma_o} \tag{4}$$

$$D_1 = \frac{m_B}{m_S} = B_c \tag{5}$$

$$D_2 = \frac{m_W}{m_S} = w_c^M (1 + B_c) \tag{6}$$

$$D_3 = S_a^M T_c \sqrt{\rho_d^M \sigma_o} \tag{7}$$

where D_o = dependent/output dimensionless variable (or the stress ratio), which is intended to be modeled; D_1, D_2 and D_3 = independent/input dimensionless variables; B_c = binder (or cement) content; and w_c^M = initial or as-compacted water content of the mixture composite.

As outlined in Section 2, for each dataset or soil type, the natural soil and its various cemented blends were molded and further tested for UCS at their respective standard or modified Proctor optimum condition; the molding dry densities and water contents are provided in Table A2 of the Appendix A section. As for S_a^M, the weighted averaging technique, as commonly adopted in the research literature, was employed to arrive at an estimate of the mixture's initial specific surface area [23,32,59]:

$$S_a^M = (1 - B_c) S_a^S + B_c S_a^B \tag{8}$$

where S_a^S = specific surface area of the natural soil; and S_a^B = specific surface area of the cementitious binder.

In the absence of S_a^S measurements, which was the case for all datasets compiled in the present study, the following empirical relationship was used to estimate the natural soil's specific surface area (in m^2/g) [23,59,63]:

$$S_a^S = f_c (\tfrac{10}{7} I_P + 5) \tag{9}$$

where f_c = fines content (< 75 μm) of the natural soil; and I_P = plasticity index of the natural soil (in %).

The only remaining unknown in Equation (8) is S_a^B, which was either reported as part of the original data source or was taken from relevant literature sources [64]. The S_a^S (obtained as per Equation (9)), S_a^B and S_a^M (obtained as per Equation (8)) values for the compiled database of 171 UCS tests are summarized in Table A2 of the Appendix A section.

The original soil–cement UCS problem given in Equation (1) can now be rewritten as:

$$D_o = \frac{q_u}{\sigma_o} = h(D_1, D_2, D_3) \tag{10}$$

where h = an unknown three-variable functional expression, which is to be obtained through trial-and-error.

To further accommodate model parsimony, any suggested functional expression for h should involve a limited number of model/fitting coefficients while retaining a simple algebraic structure. The former facilitates model calibration by minimal experimental effort, while the latter, the structural simplicity, allows for the model coefficients to be quantified by means of simple, explicit calculations. It is well accepted that a standard ad-hoc solution to h is non-existent; however, one of the more common, yet simple solutions, which is also supported by the authors' previous experience, includes the multivariable power function [32,36,61]. For the soil–cement UCS problem given in Equation (10), the multivariable power function results in the following:

$$D_o = \frac{q_u}{\sigma_o} = \beta_o D_1^{\beta_1} D_2^{\beta_2} D_3^{\beta_3} \tag{11}$$

where β_o, β_1, β_2 and β_3 = model coefficients (dimensionless).

To accommodate mathematical singularities, in this case division by zero, each of the independent/input dimensionless variables, while retaining their dimensionless nature, should be mathematically manipulated [55,58]. Routine manipulations for D_x ($x \in \mathbb{N}$), as commonly practiced in the research literature, include $D_x + y$, $D_x \times y$ and D_x^y ($y \in \mathbb{R}$) [32,36,61]. For those soil–cement blends involving no binder, the natural soil, D_1 is equal to zero; as such, D_1 was changed to $P_1 = 1 - D_1$. Moreover, the curing time for the natural soil, despite being zero, was assumed to be at least $T_c = 1$ days; this was to accommodate singularities encountered in D_3. Through trial-and-error, the model coefficients with respect to D_2 and D_3 were found to be approximately equal, i.e., $\beta_2 \approx \beta_3$. As such, D_2 and D_3 were unified into a new independent dimensionless variable with a new power exponent, i.e., $P_2 = D_2D_3$ with a power exponent of $\beta_2^* = \beta_2 \approx \beta_3$. This simplification reduces the number of model coefficients and hence makes for a simpler calibration procedure. In view of the aforementioned considerations, Equation (11) can now be expressed as:

$$D_o = \frac{q_u}{\sigma_o} = \beta_o P_1^{\beta_1} P_2^{\beta_2^*} \tag{12}$$

In terms of graphical representation, the proposed dimensional model given in Equation (12) resembles a curved surface in the three-dimensional space of D_o:P_2:P_1. As typical cases, Figures 2a and 2b illustrate the variations of D_o against P_2 and P_1 for the datasets S_3 and S_{14}, respectively. As is evident from the contour lines outlined in the P_2:P_1 plane, both variables P_2 and P_1 strongly influence D_o and hence hold physical significance for model development. For any given P_2, an increase in P_1 led to a decrease in D_o and hence the UCS (or q_u). On the contrary, for any given P_1, the variations of D_o with respect to an increase in P_2 followed a monotonically-increasing trend. Accordingly, it can be concluded that $\beta_o > 0$, $\beta_1 < 0$ and $\beta_2^* > 0$. It should be noted that P_1 captures the effects of binder (or cement) content, while P_2 takes into account the combined effects of compaction state, hydration and curing time.

Finally, substituting Equations (4) to (7) into Equation (12) results in the following relationship for the UCS:

$$q_u = \beta_o \sigma_o (1 - B_c)^{\beta_1} \left[w_c{}^{M} S_a{}^{M} T_c (1 + B_c) \sqrt{\rho_d{}^{M} \sigma_o} \right]^{\beta_2^*} \tag{13}$$

3.2. Model Performance

The proposed dimensional model given in Equation (13) was fitted to the experimental UCS data (presented in Figure A1 of the Appendix A section) by means of the non-linear least-squares optimization technique. Routine statistical tests, namely Fisher's *F*-test and Student's *t*-test, were then carried out (at α = 5% significance level) to examine the model's statistical significance. The *F*-test sheds light on the model's overall significance, while the *t*-test examines the significance of the independent/input regression components, i.e., $P_1 = 1 - D_1$ and $P_2 = D_2D_3$ [1]. In addition, statistical fit-measure indices — including the coefficient of determination R^2 (dimensionless), the root-mean-squared error RMSE (in kPa), and the normalized root-mean-squared error NRMSE (in %) — were used to assess the model's predictive capability [32,61]:

$$\text{RMSE} = \sqrt{\frac{1}{N^*} \sum_{i=1}^{N^*} \left[\left(q_u{}^{A}\right)_i - \left(q_u{}^{P}\right)_i \right]^2} \tag{14}$$

$$\text{NRMSE} = \frac{\text{RMSE}}{\left(q_u{}^{A}\right)_{\max} - \left(q_u{}^{A}\right)_{\min}} \times 100\% \tag{15}$$

where q_u^A = actual UCS (in kPa), as presented in Figure A1 of the Appendix A section; q_u^P = predicted UCS (in kPa), obtained as per Equation (13); i = index of summation; and N^* = number of experimental UCS data in each dataset (see Table A2).

The regression analysis outputs with respect to Equation (13) are summarized in Table 1. As typical cases, Figures 3a and 3b illustrate the variations of predicted against actual UCS data, along with the corresponding 95% prediction bands/intervals, for the datasets S_3 and S_{14}, respectively. The high R^2 and low RMSE or NRMSE values warrant a strong agreement between the actual and predicted UCS data, both in terms of correlation and error. The R^2 values were unanimously greater than 0.95, thus indicating that leastwise, 95% of the variations in experimental observations are captured and further explained by the proposed dimensional model. In terms of forecast error, the NRMSE was found to be less than 5% for the majority of cases, hence indicating a maximum offset of 5% associated with the predictions. The p-values associated with Fisher's F-test were unanimously less than 5%, thus corroborating the model's overall statistical significance with a 95% confidence level. Similarly, for Student's t-test, the p-values associated with the independent regression components, i.e., P_1 and P_2, were found to be less than 5% for all datasets, hence implying that these dimensionless variables are statistically significant and hence effectively contribute towards the predictions.

Figure 4a illustrates the variations of predicted, by Equation (13), against actual UCS data, along with the corresponding 95% prediction bands, for the compiled database of 171 natural and cement-treated samples. Despite the existence of some scatter, all data points cluster around the line of equality, i.e., $y = x$, and position themselves between the 95% lower and upper prediction bands, indicating no particular outliers associated with the predictions. The R^2 and NRMSE indices were also calculated for these combined datasets, which resulted in a net R^2 and a net NRMSE of 0.981 and 2.38%, respectively. A common benchmark for soil–cement UCS modelling, as reported in the research literature, is the use of multiple linear regression (MLR) analysis [1,25,26,65]. For a given soil type blended with cement, a suitable MLR model can be given as:

$$q_u = \alpha_o + \alpha_1 B_c + \alpha_2 T_c \tag{16}$$

where α_o, α_1 and α_2 = model coefficients (obtained by means of the linear least-squares optimization technique); and α_o = UCS of the natural soil, since setting $B_c = 0$ and $T_c = 0$ leads to $q_u = \alpha_o$.

The variations of predicted, by Equation (16), against actual UCS data for the compiled database of 171 natural and cement-treated samples are provided in Figure 4b. In comparison to the proposed dimensional model or Equation (13), the MLR model was found to exhibit an increased level of scattering (compare Figures 4a and 4b). The MLR model resulted in a net R^2 and a net NRMSE of 0.919 and 6.75%, respectively. These values indicate an inferior performance compared with the proposed dimensional model, which exhibited a notably higher R^2 (of 0.981) and a relatively lower NRMSE (of 2.38%). More importantly, as depicted in Figure 4b, the MLR model was found to promote negative predictions in some cases (e.g., S_5 and S_{13} where $B_c = 0$ and $T_c = 0$), thus implying that the conventional MLR approach, though statistically significant, does not hold physical significance/meaning.

3.3. Sensetivity Analysis

The partial derivative sensitivity analysis technique, as commonly adopted in the research literature [1,62,65], was carried out on Equation (13) to quantify the relative impacts of binder (or cement) content B_c, curing time T_c and soil plasticity on the UCS. For this purpose, the fifteen soil types (or datasets) were divided into three plasticity classes based on their liquid limit w_L: (**i**) low plasticity (w_L < 35%) consisting of S_3, S_{13} and S_{15}; (**ii**) intermediate plasticity (35% < w_L < 50%) consisting of S_2, S_4–S_8 and S_{10}; and (**iii**) high plasticity (w_L > 50%) consisting of S_1, S_9, S_{11}, S_{12} and S_{14}. For a given soil plasticity class, the overall/net relative impact (including both positive and negative) of $x_a = B_c$ or T_c on the UCS (or q_u), also referred to as sensitivity, can be defined as:

$$S^{\mathrm{PN}}(x_a) = \frac{\sigma(x_a)}{M^* \sigma(q_{\mathrm{u}})} \times \sum_{j=1}^{M^*} \left| d_{aj} \right| \ni d_a = \frac{\partial q_{\mathrm{u}}}{\partial x_a} \tag{17}$$

where d_a = partial derivative of q_u, i.e., Equation (12) or (13), with respect to $x_a = B_c$ or T_c (see the footer of Table 2); $\sigma(x_a)$ = standard deviation of x_a data; $\sigma(q_u)$ = standard deviation of predicted q_u data; j = index of summation; and M^* = number of observations (or data points) in each soil plasticity class (= 33, 88 and 50 for low, intermediate and highly plasticity classes, respectively).

The partial derivative term in Equation (17), i.e., $d_a = \partial q_u/\partial x_a$, measures the likelihood of q_u increasing or decreasing as a result of an increase in x_a. Accordingly, the positive and negative impacts of $x_a = B_c$ or T_c on q_u can be, respectively, defined as:

$$\forall x_a \ni d_a > 0: \ S^{\mathrm{P}}(x_a) = \frac{\sigma(x_a)}{M^* \sigma(q_{\mathrm{u}})} \times \sum_{j=1}^{M^*} \left| d_{aj} \right| \ni d_a = \frac{\partial q_{\mathrm{u}}}{\partial x_a} \tag{18}$$

$$\forall x_a \ni d_a < 0: \ S^{\mathrm{N}}(x_a) = \frac{\sigma(x_a)}{M^* \sigma(q_{\mathrm{u}})} \times \sum_{j=1}^{M^*} \left| d_{aj} \right| \ni d_a = \frac{\partial q_{\mathrm{u}}}{\partial x_a} \tag{19}$$

It should be noted that $S^P(x_a)$ (Equation (18)) and $S^N(x_a)$ (Equation (19)) are, respectively, positive and negative fractions of the sensitivity parameter $S^{PN}(x_a)$ (Equation (17)), meaning that $S^{PN}(x_a) = S^P(x_a) + S^N(x_a)$. Quite clearly, the main objective of any introduced soil stabilization scheme, in this case cement stabilization, is to promote an increase in the UCS. Accordingly, the variations of the positive sensitivity parameter, i.e., $S^P(x_a)$ or Equation (18), would be of interest for further analyses. To facilitate a more practical comparison, the positive sensitivity parameter can also be expressed in terms of percentage [1]:

$$S^{\mathrm{P}\%}(x_a) = \frac{S^{\mathrm{P}}(x_a)}{\sum_{a=1}^{K^*} S^{\mathrm{P}}(x_a)} \times 100\% \tag{20}$$

where $S^{P\%}(x_a)$ = positive contribution offered by an increase in $x_a = B_c$ or T_c leading to an increase in q_u (in %); a = index of summation; and K^* = number of independent variables (= 2, namely B_c and T_c).

The sensitivity analysis results with respect to Equation (13) are summarized in Table 2. As expected, for all three plasticity classes, the negative sensitivity parameter with respect to both B_c and T_c was found to be zero, i.e., $S^N(B_c) = S^N(T_c) = 0$. Accordingly, the likelihood of increase in the UCS as a result of an increase in B_c and/or T_c can be taken as 100%, thus implying that cement stabilization, regardless of soil plasticity, consistently leads to favorable UCS improvements which can be further enhanced by means of curing. For all three soil groups, the positive sensitivity parameter with respect to B_c was found to be greater than that of T_c, i.e., $S^P(B_c) > S^P(T_c)$. As such, regardless of soil plasticity, the positive contribution offered by an increase in binder content resulting in an increase in the UCS is more dominant compared with that of curing time. Interestingly, the higher the soil plasticity, the higher the positive sensitivity to binder content — that is, $S^P(B_c)$ = 0.64, 0.86 and 1.13 for low, intermediate and high plasticity classes, respectively. Hence, it can be concluded that soils of higher plasticity would potentially require higher binder contents for stabilization. On the contrary, the higher the soil plasticity, the lower the positive sensitivity to curing time, thus indicating a more effective cement hydration process in soils of lower plasticity — that is, an increase in the soil's clay and silt contents, which are hydrophilic in nature, deprives cement grains from easy access to water and hence delays and/or hinders cement hydration [23].

3.4. Model Calibration

The proposed dimensional model given in Equation (12) or (13) contains a total of three model coefficients, namely β_o, β_1 and β_2^*. These coefficients can be calibrated by means of typical soil–cement UCS tests, thereby allowing for the dimensional model to be implemented for predictive purposes and/or soil–cement optimization studies. The three model coefficients can be adequately calibrated by a total of three UCS tests. Recommended mix designs for the three UCS tests include the natural soil, i.e., $B_c = 0$ and $T_c = 1$ days, and an arbitrary soil–cement blend at two different curing times. In general, the choices of binder content and curing times for the soil–cement blend are arbitrary. From a statistical perspective, however, a desired maximum binder content (denoted as B_c^H), tested at both short (denoted as T_c^L) and long (denoted as T_c^H) curing conditions, is expected to yield a more reliable estimate of the model coefficients. This can be attributed to the monotonically-increasing trend of the UCS with respect to both the binder content and the curing time (see Figure A1). For the dataset S_{10}, for instance, suitable inputs can be taken as $B_c^H = 9\%$, $T_c^L = 3$ days and $T_c^H = 28$ days (see Table A2). Assuming that the three required UCS data are at hand, the following system of three semi-linear equations should be solved to arrive at an estimate of the model coefficients β_o, β_1 and β_2^*:

$$\begin{cases} \mathrm{Ln}\left[\dfrac{q_u(0,1)}{\sigma_o}\right] = \mathrm{Ln}\left[\beta_o\right] + \beta_1 \mathrm{Ln}\left[P_1(0,1)\right] + \beta_2^* \mathrm{Ln}\left[P_2(0,1)\right] \\ \mathrm{Ln}\left[\dfrac{q_u(B_c^H, T_c^L)}{\sigma_o}\right] = \mathrm{Ln}\left[\beta_o\right] + \beta_1 \mathrm{Ln}\left[P_1(B_c^H, T_c^L)\right] + \beta_2^* \mathrm{Ln}\left[P_2(B_c^H, T_c^L)\right] \\ \mathrm{Ln}\left[\dfrac{q_u(B_c^H, T_c^H)}{\sigma_o}\right] = \mathrm{Ln}\left[\beta_o\right] + \beta_1 \mathrm{Ln}\left[P_1(B_c^H, T_c^H)\right] + \beta_2^* \mathrm{Ln}\left[P_2(B_c^H, T_c^H)\right] \end{cases} \quad (21)$$

where $q_u(0,1)$ = actual UCS for $B_c = 0$ and $T_c = 1$ days (natural soil); $P_1(0,1)$ and $P_2(0,1)$ = first and second independent dimensionless variables for $B_c = 0$ and $T_c = 1$ days; $q_u(B_c^H,T_c^L)$ = actual UCS for $B_c = B_c^H$ and $T_c = T_c^L$; $P_1(B_c^H,T_c^L)$ and $P_2(B_c^H,T_c^L)$ = first and second independent dimensionless variables for $B_c = B_c^H$ and $T_c = T_c^L$; $q_u(B_c^H,T_c^H)$ = actual UCS for $B_c = B_c^H$ and $T_c = T_c^H$; and $P_1(B_c^H,T_c^H)$ and $P_2(B_c^H,T_c^H)$ = first and second independent dimensionless variables for $B_c = B_c^H$ and $T_c = T_c^H$.

The explicit solution to Equation (21) is given in Equation (B3) of the Appendix B section. To examine the suggested calibration procedure in terms of cogency, the three model coefficients and hence the formerly-predicted UCS data (outlined in Figure 4a) were first recalculated for each of the fifteen soil–cement datasets based on three actual UCS measurements — that is, $q_u(0,1)$, $q_u(B_c^H,T_c^L)$ and $q_u(B_c^H,T_c^H)$, as selected in Appendix A. The newly-predicted UCS data were then plotted against their formerly-predicted counterparts, and the results are provided in Figure 5a. The high R^2 (= 0.975) and low RMSE or NRMSE (= 2.88%) indices warrant a strong agreement between the newly- and formerly-predicted UCS data, and thus validate the suggested calibration procedure outlined in Equation (21). Figure 5b illustrates the variations of the newly-predicted against actual UCS data, along with the corresponding 95% prediction bands, for the compiled database of 171 natural and cement-treated samples. Despite the existence of a more notable scatter compared with that of Figure 4a, no major outliers were associated with the new predictions. Moreover, the fit-measure indices with respect to Figure 5b were calculated as $R^2 = 0.956$ and NRMSE = 3.68%, both of which are on par with those reported in Figure 4a, i.e., $R^2 = 0.981$ and NRMSE = 2.38%; these results provide further verification for the suggested calibration procedure.

4. Concluding Remarks

The dimensional analysis concept was successfully extended to the soil–cement UCS problem, thereby leading to the development of a practical dimensional model capable of simulating the UCS of compacted soil–cement blends as a function of the composite's index properties — that is, binder (or cement) content, specific surface area, curing time, and the compaction/molding state parameters, namely water content and dry density (or void ratio). The predictive capability of the proposed dimensional model was examined and further validated by means of routine statistical tests, as well as conventional fit-measure indices. A sensitivity analysis was also carried out to quantify the relative impacts of the model's input variables, namely binder content, curing time and soil plasticity, on the UCS. The results indicated that the higher the soil plasticity, the higher the positive sensitivity to binder content, thus implying that soils of higher plasticity would potentially require higher binder contents for stabilization. On the contrary, the higher the soil plasticity, the lower the positive sensitivity to curing time, hence indicating a more effective cement hydration process in soils of lower plasticity.

An explicit calibration procedure, involving a total of three UCS measurements for three recommended soil–cement mix designs, was also proposed and validated, thus allowing for the proposed dimensional model to be implemented with confidence for predictive purposes, preliminary design assessments and/or soil–cement optimization studies. The three model coefficients, particularly β_1 and β_2^*, were found to be dependent on the type of soil and hence may be correlated with the soils' intrinsic properties, including (but not limited to) the consistency limits (e.g., liquid limit and plasticity index) and the free swell ratio (i.e., a quantitative measure of soil mineralogy). Such correlations were not apparent in the present study, as the compiled database was rather inconsistent in terms of the adopted sample preparation technique, as well as the implemented UCS testing procedure (e.g., loading rate). Therefore, a systematically-controlled test program should be carried out to explore casual links/correlations between the model coefficients and the soils' intrinsic properties.

It should be noted that the proposed dimensional model is valid only when the natural soil (no binder) and its various cemented blends are compacted at their respective standard or modified Proctor optimum condition, which is often implemented in practice. Additional UCS tests at wet and dry of standard and/or modified Proctor optimum conditions should be carried out to derive a more generalized model capable of simulating the UCS at varying initial placement conditions. Finally, a systematically-controlled test program can be carried out to incorporate additional physical parameters representing real-life field conditions — such as mellowing time, curing temperature, and relative humidity during curing — into the dimensional analysis, thus allowing to simulate the mechanical performance of soil–cement under local environmental fluctuations.

Disclosure Statement: This research did not receive any specific grant from funding agencies in the public, commercial, or not-for-profit sectors. The authors declare no conflict of interest.

Appendix A

As outlined in Section 2, the compiled soil–cement database consisted of fifteen fine-grained soils, i.e., S_1 to S_{15}, of varying geological and mineralogical origins, gradations and plasticity features, each tested for UCS at varying binder (or cement) contents (i.e., binder-to-soil mass ratio) and curing times. Table A1 presents a detailed description of the natural soils' (no binder) grain-size distribution, plasticity features, and corresponding USCS classifications. Moreover, relevant details with regards to the implemented testing scheme for each dataset — including the selected compaction/molding states, and the binder properties (e.g., type of cement, its content and specific surface area) — are summarized in Table A2. Finally, Figure A1 illustrates the variations of the reported UCS data against curing time for the fifteen soil–cement datasets outlined in Table A2.

Appendix B

The system of three semi-linear equations given in Equation (21) can be represented in matrix form — that is, A**X** = B where **X** is a one-by-three matrix representing the model coefficients β_o, β_1 and β_2^* — by the following relationship:

$$\begin{bmatrix} 1 & \mathrm{Ln}\left[P_1(0,1)\right] & \mathrm{Ln}\left[P_2(0,1)\right] \\ 1 & \mathrm{Ln}\left[P_1(B_c{}^{H},T_c{}^{L})\right] & \mathrm{Ln}\left[P_2(B_c{}^{H},T_c{}^{L})\right] \\ 1 & \mathrm{Ln}\left[P_1(B_c{}^{H},T_c{}^{H})\right] & \mathrm{Ln}\left[P_2(B_c{}^{H},T_c{}^{H})\right] \end{bmatrix} \times \begin{bmatrix} \mathrm{Ln}\left[\beta_o\right] \\ \beta_1 \\ \beta_2{}^{*} \end{bmatrix} = \begin{bmatrix} \mathrm{Ln}\left[\dfrac{q_u(0,1)}{\sigma_o}\right] \\ \mathrm{Ln}\left[\dfrac{q_u(B_c{}^{H},T_c{}^{L})}{\sigma_o}\right] \\ \mathrm{Ln}\left[\dfrac{q_u(B_c{}^{H},T_c{}^{H})}{\sigma_o}\right] \end{bmatrix} \tag{B1}$$

For ease of presentation, Equation (B1) is expressed as:

$$\begin{bmatrix} a_{11} & a_{12} & a_{13} \\ a_{21} & a_{22} & a_{23} \\ a_{31} & a_{32} & a_{33} \end{bmatrix} \times \begin{bmatrix} \mathrm{Ln}\left[\beta_o\right] \\ \beta_1 \\ \beta_2{}^{*} \end{bmatrix} = \begin{bmatrix} b_{11} \\ b_{21} \\ b_{31} \end{bmatrix} \tag{B2}$$

The explicit solution to Equation (B2), defined as **X** = $A^{-1}B$, can be given as:

$$\begin{cases} \beta_o = \exp\left[\dfrac{a_{12}(b_{31}a_{23}-b_{21}a_{33})+a_{22}(b_{11}a_{33}-b_{31}a_{13})+a_{32}(b_{21}a_{13}-b_{11}a_{23})}{a_{12}(a_{23}-a_{33})+a_{22}(a_{33}-a_{13})+a_{32}(a_{13}-a_{23})}\right] \\ \beta_1 = \dfrac{a_{13}(b_{31}-b_{21})+a_{23}(b_{11}-b_{31})+a_{33}(b_{21}-b_{11})}{a_{12}(a_{23}-a_{33})+a_{22}(a_{33}-a_{13})+a_{32}(a_{13}-a_{23})} \\ \beta_2{}^{*} = \dfrac{a_{12}(b_{21}-b_{31})+a_{22}(b_{31}-b_{11})+a_{32}(b_{11}-b_{21})}{a_{12}(a_{23}-a_{33})+a_{22}(a_{33}-a_{13})+a_{32}(a_{13}-a_{23})} \end{cases} \tag{B3}$$

References

[1] Zhang J, Soltani A, Deng A, et al. Mechanical performance of jute fiber-reinforced micaceous clay composites treated with ground-granulated blast-furnace slag. *Materials.* **2019**;12:576. https://doi.org/10.3390/ma12040576

[2] Petry TM, Little DN. Review of stabilization of clays and expansive soils in pavements and lightly loaded structures—history, practice, and future. *J. Mater. Civ. Eng.* **2002**;14:447–460. https://doi.org/10.1061/(asce)0899-1561(2002)14:6(447)

[3] Soltani A, Deng A, Taheri A, et al. Swell–shrink behavior of rubberized expansive clays during alternate wetting and drying. *Minerals.* **2019**;9:224. https://doi.org/10.3390/min9040224

[4] Winterkorn HF, Pamukcu S. Soil stabilization and grouting. In: Fang HY, editor. *Foundation Engineering Handbook.* 2nd ed. Boston, MA, USA: Springer; **1991**. p. 317–378. https://doi.org/10.1007/978-1-4615-3928-5_9, ISBN:9781461539285

[5] Soltani A, Taheri A, Khatibi M, et al. Swelling potential of a stabilized expansive soil: a comparative experimental study. *Geotech. Geol. Eng.* **2017**;35:1717–1744. https://doi.org/10.1007/s10706-017-0204-1

[6] Hejazi SM, Sheikhzadeh M, Abtahi SM, et al. A simple review of soil reinforcement by using natural and synthetic fibers. *Constr. Build. Mater.* **2012**;30:100–116. https://doi.org/10.1016/j.conbuildmat.2011.11.045

[7] Mirzababaei M, Miraftab M, Mohamed M, et al. Unconfined compression strength of reinforced clays with carpet waste fibers. *J. Geotech. Geoenviron. Eng.* **2013**;139:483–493. https://doi.org/10.1061/(asce)gt.1943-5606.0000792

[8] Kutanaei SS, Choobbasti AJ. Triaxial behavior of fiber-reinforced cemented sand. *J. Adhes. Sci. Technol.* **2016**;30:579–593. https://doi.org/10.1080/01694243.2015.1110073

[9] Choobbasti AJ, Kutanaei SS. Effect of fiber reinforcement on deformability properties of cemented sand. *J. Adhes. Sci. Technol.* **2017**;31:1576–1590. https://doi.org/10.1080/01694243.2016.1264681

[10] Gowthaman S, Nakashima K, Kawasaki S. A state-of-the-art review on soil reinforcement technology using natural plant fiber materials: past findings, present trends and future directions. *Materials.* **2018**;11:553. https://doi.org/10.3390/ma11040553

[11] Ghadakpour M, Choobbasti AJ, Kutanaei SS. Investigation of the deformability properties of fiber reinforced cemented sand. *J. Adhes. Sci. Technol.* **2019**;33:1913–1938. https://doi.org/10.1080/01694243.2019.1619224

[12] Soltani A, Deng A, Taheri A, et al. Swell–shrink–consolidation behavior of rubber-reinforced expansive soils. *Geotech. Test. J.* **2019**;42:761–788. https://doi.org/10.1520/gtj20170313

[13] Estabragh AR, Naseh M, Beytolahpour I, et al. Strength of a clay soil and soil–cement mixture with resin. *Proc. Inst. Civ. Eng. Gr. Improv.* **2013**;166:108–114. https://doi.org/10.1680/grim.12.00014

[14] Firoozi AA, Olgun CG, Firoozi AA, et al. Fundamentals of soil stabilization. *Int. J. Geo-Eng.* **2017**;8:26. https://doi.org/10.1186/s40703-017-0064-9

[15] Mirzababaei M, Arulrajah A, Horpibulsuk S, et al. Stabilization of soft clay using short fibers and poly vinyl alcohol. *Geotext. Geomembranes.* **2018**;46:646–655. https://doi.org/10.1016/j.geotexmem.2018.05.001

[16] Choobbasti AJ, Samakoosh MA, Kutanaei SS. Mechanical properties soil stabilized with nano calcium carbonate and reinforced with carpet waste fibers. *Constr. Build. Mater.* **2019**;211:1094–1104. https://doi.org/10.1016/j.conbuildmat.2019.03.306

[17] Soltani A, Deng A, Taheri A, et al. A sulphonated oil for stabilisation of expansive soils. *Int. J. Pavement Eng.* **2019**;20:1285–1298. https://doi.org/10.1080/10298436.2017.1408270

[18] Soltani A, Deng A, Taheri A, et al. Engineering reactive clay systems by ground rubber replacement and polyacrylamide treatment. *Polymers.* **2019**;11:1675. https://doi.org/10.3390/polym11101675

[19] Valizadeh M, Choobbasti AJ. Evaluation of nano-graphene effect on mechanical behavior of clayey sand with microstructural and self-healing approach. *J. Adhes. Sci. Technol.* **2019**;in press:1–20. https://doi.org/10.1080/01694243.2019.1676598

[20] Horpibulsuk S, Miura N, Nagaraj TS. Clay–water/cement ratio identity for cement admixed soft clays. *J. Geotech. Geoenviron. Eng.* **2005**;131:187–192. https://doi.org/10.1061/(asce)1090-0241(2005)131:2(187)

[21] Sunitsakul J, Sawatparnich A, Sawangsuriya A. Prediction of unconfined compressive strength of soil–cement at 7 days. *Geotech. Geol. Eng.* **2012**;30:263–268. https://doi.org/10.1007/s10706-011-9460-7

[22] Horpibulsuk S, Suddeepong A, Suksiripattanapong C, et al. Water-void to cement ratio identity of lightweight cellular-cemented material. *J. Mater. Civ. Eng.* **2014**;26:6014021. https://doi.org/10.1061/(asce)mt.1943-5533.0001110

[23] Williamson S, Cortes DD. Dimensional analysis of soil–cement mixture performance. *Géotechnique Lett.* **2014**;4:33–38. https://doi.org/10.1680/geolett.13.00082

[24] Consoli NC, Ferreira PMV, Tang SC, et al. A unique relationship determining strength of silty/clayey soils—Portland cement mixes. *Soils Found.* **2016**;56:1082–1088. https://doi.org/10.1016/j.sandf.2016.11.011

[25] Abbey SJ, Ngambi S, Ganjian E. Development of strength models for prediction of unconfined compressive strength of cement/byproduct material improved soils. *Geotech. Test. J.* **2017**;40:928–935. https://doi.org/10.1520/gtj20160138

[26] Sharma LK, Singh TN. Regression-based models for the prediction of unconfined compressive strength of artificially structured soil. *Eng. Comput.* **2018**;34:175–186. https://doi.org/10.1007/s00366-017-0528-8

[27] Yapage NNS, Liyanapathirana DS. A review of constitutive models for cement-treated clay. *Int. J. Geotech. Eng.* **2019**;13:525–537. https://doi.org/10.1080/19386362.2017.1370878

[28] Alavi AH, Gandomi AH, Mollahasani A. A genetic programming-based approach for the performance characteristics assessment of stabilized soil. In: Chiong R, Weise T, Michalewicz Z, editors. *Variants of Evolutionary Algorithms for Real-World Applications.* Berlin, Germany: Springer; **2012**. p. 343–376. https://doi.org/10.1007/978-3-642-23424-8_11, ISBN:9783642234248

[29] Kutanaei SS, Choobbasti AJ. Prediction of combined effects of fibers and cement on the mechanical properties of sand using particle swarm optimization algorithm. *J. Adhes. Sci. Technol.* **2015**;29:487–501. https://doi.org/10.1080/01694243.2014.995343

[30] Suman S, Mahamaya M, Das SK. Prediction of maximum dry density and unconfined compressive strength of cement stabilised soil using artificial intelligence techniques. *Int. J. Geosynth. Gr. Eng.* **2016**;2:11. https://doi.org/10.1007/s40891-016-0051-9

[31] Choobbasti AJ, Kutanaei SS, Taslimi M, et al. Modeling of compressive strength of cemented sandy soil. *J. Adhes. Sci. Technol.* **2019**;33:791–807. https://doi.org/10.1080/01694243.2018.1548535

[32] Soltani A, Mirzababaei M. Discussion on "Effects of lime addition on geotechnical properties of sedimentary soil in Curitiba, Brazil" [J Rock Mech Geotech Eng 10 (2018) 188–194]. *J. Rock Mech. Geotech. Eng.* **2019**;11:214–218. https://doi.org/10.1016/j.jrmge.2018.08.008

[33] Buckingham E. On physically similar systems; illustrations of the use of dimensional equations. *Phys. Rev.* **1914**;4:345–376. https://doi.org/10.1103/physrev.4.345

[34] Butterfield R. Dimensional analysis for geotechnical engineers. *Géotechnique.* **1999**;49:357–366. https://doi.org/10.1680/geot.1999.49.3.357

[35] Buzzi O. On the use of dimensional analysis to predict swelling strain. *Eng. Geol.* **2010**;116:149–156. https://doi.org/10.1016/j.enggeo.2010.08.005

[36] Soltani A, Deng A, Taheri A, et al. Interfacial shear strength of rubber-reinforced clays: a dimensional analysis perspective. *Geosynth. Int.* **2019**;26:164–183. https://doi.org/10.1680/jgein.18.00045

[37] Miller GA, Azad S. Influence of soil type on stabilization with cement kiln dust. *Constr. Build. Mater.* **2000**;14:89–97. https://doi.org/10.1016/s0950-0618(00)00007-6

[38] Estabragh AR, Beytolahpour I, Javadi AA. Effect of resin on the strength of soil–cement mixture. *J. Mater. Civ. Eng.* **2011**;23:969–976. https://doi.org/10.1061/(asce)mt.1943-5533.0000252

[39] Estabragh AR, Namdar P, Javadi AA. Behavior of cement-stabilized clay reinforced with nylon fiber. *Geosynth. Int.* **2012**;19:85–92. https://doi.org/10.1680/gein.2012.19.1.85

[40] Abdi MR, Mirzaeifar H. Effects of discrete short polypropylene fibers on behavior of artificially cemented kaolinite. *Int. J. Civ. Eng.* **2016**;14:253–262. https://doi.org/10.1007/s40999-016-0022-5

[41] Estabragh AR, Khatibi M, Javadi AA. Effect of cement on treatment of a clay soil contaminated with glycerol. *J. Mater. Civ. Eng.* **2016**;28:04015157. https://doi.org/10.1061/(asce)mt.1943-5533.0001443

[42] Estabragh AR, Khatibi M, Javadi AA. Effect of cement on mechanical behavior of soil contaminated with monoethylene glycol (MEG). *ACI Mater. J.* **2016**;113:709–717. https://doi.org/10.14359/51689236

[43] Chegenizadeh A, Keramatikerman M, Panizza S, et al. Effect of powdered recycled tire on sulfate resistance of cemented clay. *J. Mater. Civ. Eng.* **2017**;29:04017160. https://doi.org/10.1061/(asce)mt.1943-5533.0002011

[44] Estabragh AR, Ranjbari S, Javadi AA. Properties of clay soil and soil cement reinforced with polypropylene fibers. *ACI Mater. J.* **2017**;114:195–205. https://doi.org/10.14359/51689469

[45] Zhang CL, Jiang GL, Su LJ, et al. Effect of cement on the stabilization of loess. *J. Mt. Sci.* **2017**;14:2325–2336. https://doi.org/10.1007/s11629-017-4365-4

[46] Phanikumar BR, Nagaraju TV. Engineering behaviour of expansive clays blended with cement and GGBS. *Proc. Inst. Civ. Eng. Gr. Improv.* **2018**;171:167–173. https://doi.org/10.1680/jgrim.17.00054

[47] Yadav JS, Tiwari SK. Evaluation of the strength characteristics of cement-stabilized clay–crumb rubber mixtures for its sustainable use in geotechnical applications. *Environ. Dev. Sustain.* **2018**;20:1961–1985. https://doi.org/10.1007/s10668-017-9972-2

[48] ASTM D2487. *Standard Practice for Classification of Soils for Engineering Purposes (Unified Soil Classification System).* West Conshohocken, PA, USA: ASTM International; **2017**. https://doi.org/10.1520/d2487-17

[49] Zhao Y, Taheri A, Soltani A, et al. Strength development and strain localization behavior of cemented paste backfills using Portland cement and fly ash. *Materials.* **2019**;12:3282. https://doi.org/10.3390/ma12203282

[50] Sivapullaiah PV., Prashanth JP, Sridharan A. Effect of fly ash on the index properties of black cotton soil. *Soils Found.* **1996**;36:97–103. https://doi.org/10.3208/sandf.36.97

[51] Zhao Y, Soltani A, Taheri A, et al. Application of slag–cement and fly ash for strength development in cemented paste backfills. *Minerals.* **2019**;9:22. https://doi.org/10.3390/min9010022

[52] Grim RE. *Clay Mineralogy.* 1st ed. New York, NY, USA: McGraw-Hill; **1953**. p. 126–155.

[53] Mallela J, Von Quintus H, Smith KL. *Consideration of Lime-Stabilized Layers in Mechanistic-Empirical Pavement Design.* Arlington, VA, USA: The National Lime Association; **2004**. Available from: https://lime.org/documents/other/MechEmpPavement.pdf

[54] Sharma AK, Sivapullaiah PV. Ground granulated blast furnace slag amended fly ash as an expansive soil stabilizer. *Soils Found.* **2016**;56:205–212. https://doi.org/10.1016/j.sandf.2016.02.004

[55] Simon V, Weigand B, Gomaa H. *Dimensional Analysis for Engineers.* 1st ed. Gewerbestrasse, Cham, Switzerland: Springer; **2017**. https://doi.org/10.1007/978-3-319-52028-5, ISBN:9783319520285

[56] Johari A, Habibagahi G, Ghahramani A. Prediction of soil–water characteristic curve using genetic programming. *J. Geotech. Geoenviron. Eng.* **2006**;132:661–665. https://doi.org/10.1061/(asce)1090-0241(2006)132:5(661)

[57] Malaya C, Sreedeep S. A laboratory procedure for measuring high soil suction. *Geotech. Test. J.* **2011**;34:396–405. https://doi.org/10.1520/gtj103613

[58] Buzzi O, Giacomini A, Fityus S. Towards a dimensionless description of soil swelling behaviour. *Géotechnique.* **2011**;61:271–277. https://doi.org/10.1680/geot.7.00194

[59] Zhao Y, Gao Y, Zhang Y, et al. Effect of fines on the mechanical properties of composite soil stabilizer-stabilized gravel soil. *Constr. Build. Mater.* **2016**;126:701–710. https://doi.org/10.1016/j.conbuildmat.2016.09.082

[60] Berrah Y, Boumezbeur A, Kherici N, et al. Application of dimensional analysis and regression tools to estimate swell pressure of expansive soil in Tebessa (Algeria). *Bull. Eng. Geol. Environ.* **2018**;77:1155–1165. https://doi.org/10.1007/s10064-016-0973-4

[61] Soltani A, Mirzababaei M. Discussion of "Compaction and strength behavior of tire crumbles–fly ash mixed with clay" by Akash Priyadarshee, Arvind Kumar, Deepak Gupta, and Pankaj Pushkarna. *J. Mater. Civ. Eng.* **2019**;31:07019004. https://doi.org/10.1061/(asce)mt.1943-5533.0002701

[62] Soltani A, Estabragh AR, Taheri A, et al. Experiments and dimensional analysis of contaminated clay soils. *Environ. Geotech.* **2019**;6:434–449. https://doi.org/10.1680/jenge.18.00018

[63] Locat J, Lefebvre G, Ballivy G. Mineralogy, chemistry, and physical properties interrelationships of some sensitive clays from Eastern Canada. *Can. Geotech. J.* **1984**;21:530–540. https://doi.org/10.1139/t84-055

[64] Kosmatka SH, Kerkhoff B, Panarese WC. Portland, blended, and other hydraulic cements. *Design and Control of Concrete Mixtures, Engineering Bulletin 001.* 14th ed. Skokie, IL, USA: Portland Cement Association; **2002**. p. 21–56. ISBN:0893122173

[65] Tran KQ, Satomi T, Takahashi H. Improvement of mechanical behavior of cemented soil reinforced with waste cornsilk fibers. *Constr. Build. Mater.* **2018**;178:204–210. https://doi.org/10.1016/j.conbuildmat.2018.05.104

List of Figures

Main Text

Appendix A

Figure 1. Location of the fifteen natural soil samples (no binder), i.e., S_1 to S_{15}, on Casagrande's plasticity chart.

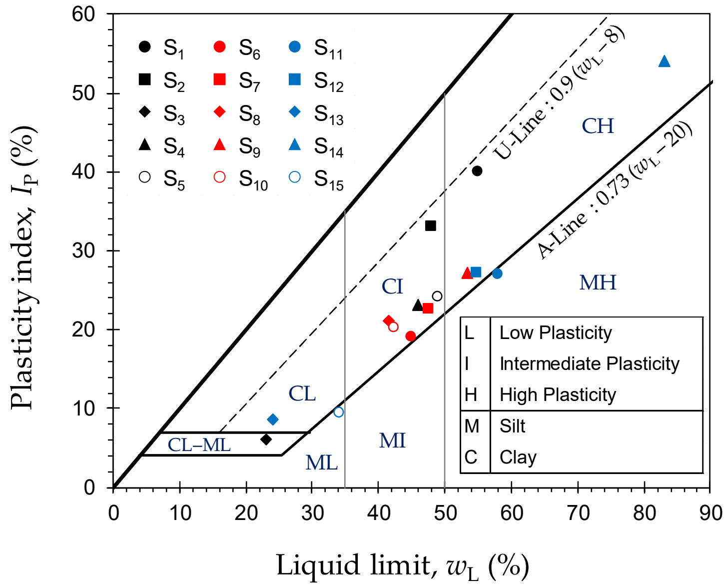

Soil	w_L (%)	I_P (%)	USCS Classification	Reference
S_1	55.0	40.0	CH (Fat Clay)	[37]
S_2	48.0	33.0	CI (Lean Clay)	[37]
S_3	23.0	6.0	CL–ML (Sandy Silty Clay)	[37]
S_4	46.0	23.0	CI (Lean Clay)	[38]
S_5	49.0	24.0	CI (Lean Clay)	[39]
S_6	45.0	19.0	CI (Lean Clay)	[40]
S_7	47.5	22.6	CI (Lean Clay with Sand)	[41]
S_8	41.5	21.1	CI (Lean Clay with Sand)	[41]
S_9	53.3	27.2	CH (Sandy Fat Clay)	[42]
S_{10}	42.4	20.2	CI (Sandy Lean Clay)	[42]
S_{11}	58.0	27.0	MH (Elastic Silt)	[43]
S_{12}	54.8	27.2	CH (Sandy Fat Clay)	[44]
S_{13}	24.0	8.5	CL (Lean Clay with Sand)	[45]
S_{14}	83.0	54.0	CH (Fat Clay)	[46]
S_{15}	34.2	9.4	ML (Silt)	[47]

Figure 2. Graphical representation of the proposed dimensional model or Equation (12) in the three-dimensional space of D_o:P_2:P_1: (**a**) S_3; and (**b**) S_{14}.

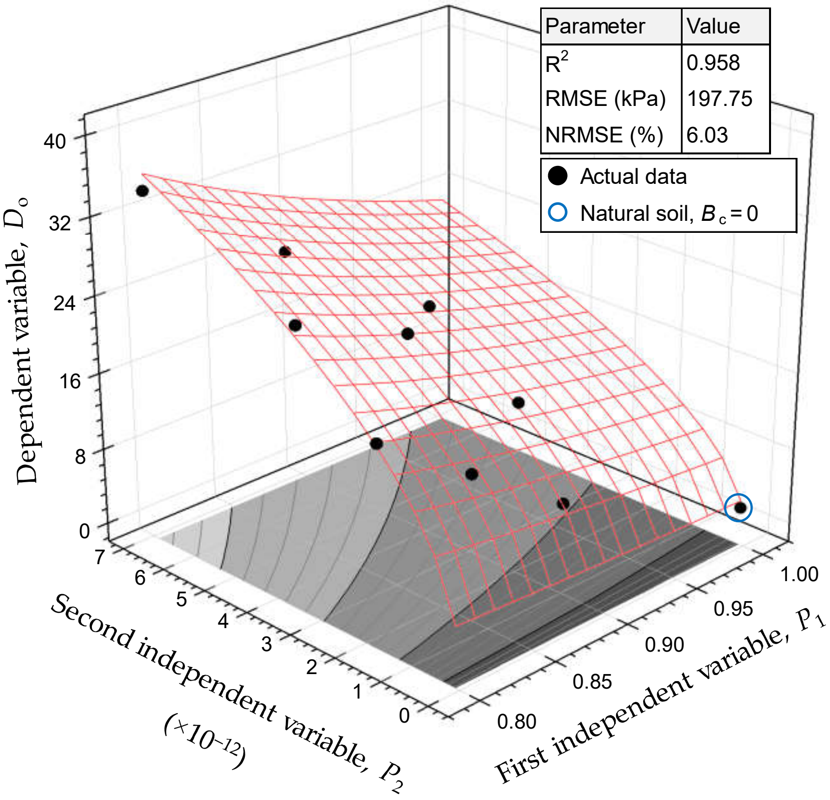

(a)

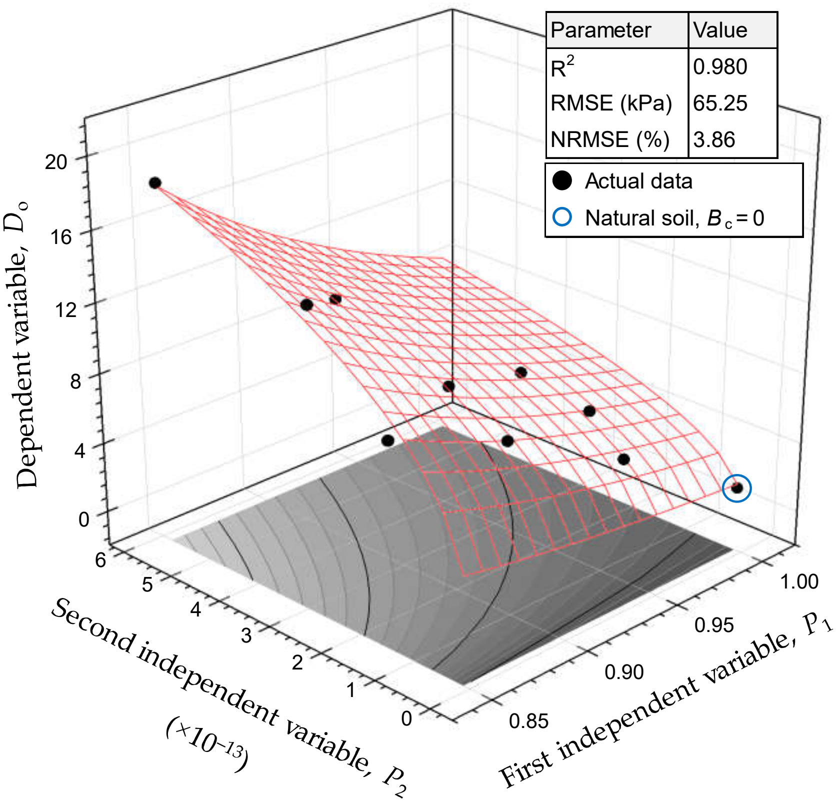

(b)

Figure 3. Variations of predicted, by Equation (13), against actual UCS data: (**a**) S_3; and (**b**) S_{14}.

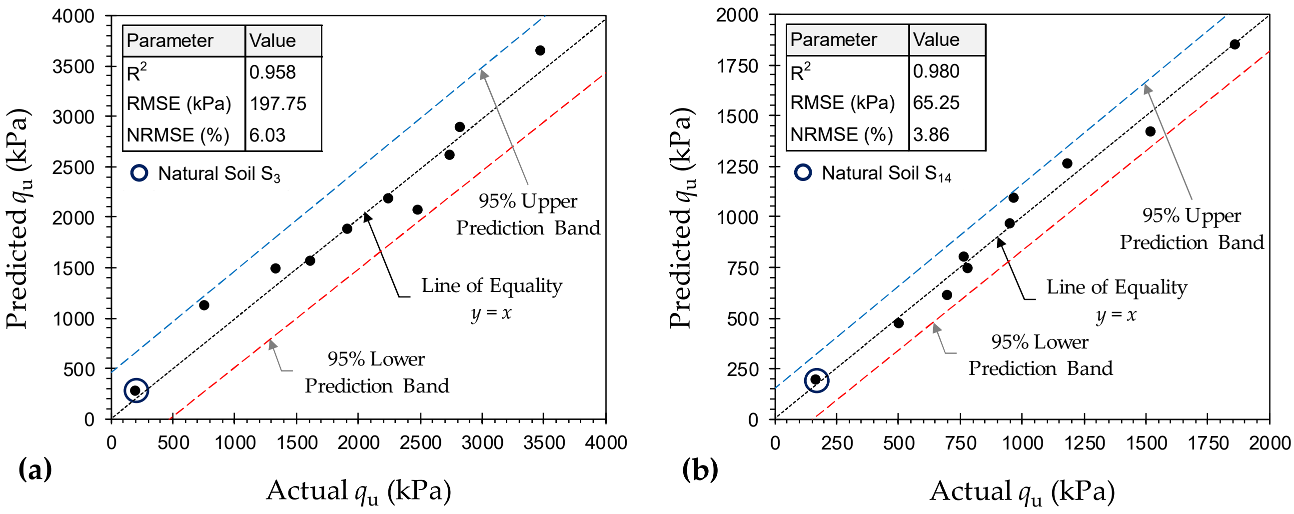

Figure 4. Variations of predicted against actual UCS data, along with the corresponding 95% prediction bands, for the compiled database of 171 natural and cement-treated samples: (**a**) Proposed dimensional model or Equation (13); and (**b**) Conventional MLR model or Equation (16).

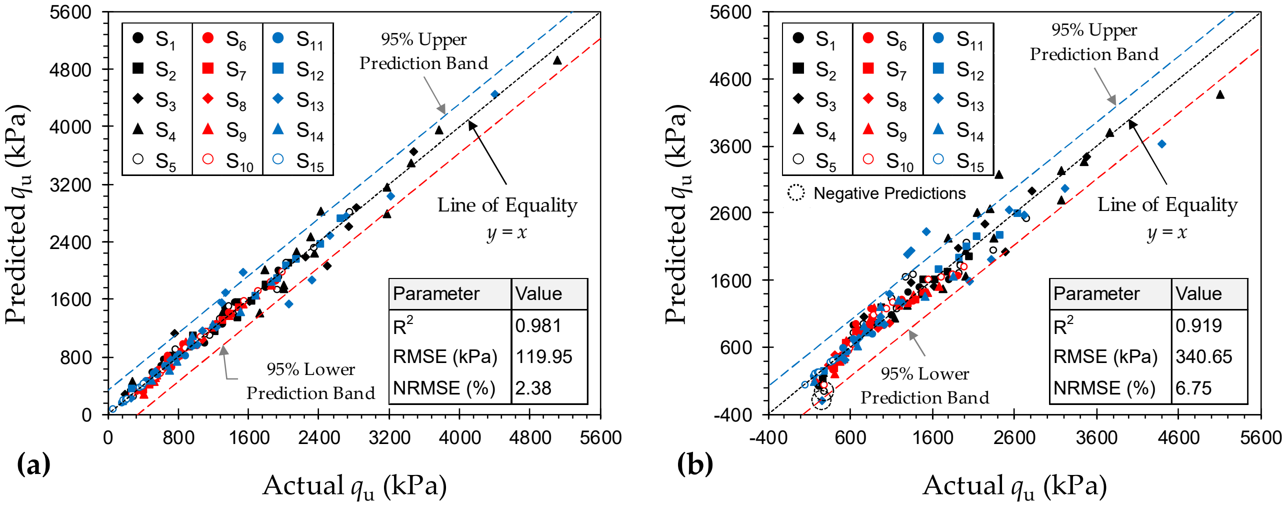

Figure 5. Variations of the newly-predicted UCS data — obtained as per the suggested calibration procedure outlined in Equation (21) — against (**a**) their formerly-predicted counterparts, and (**b**) actual UCS data.

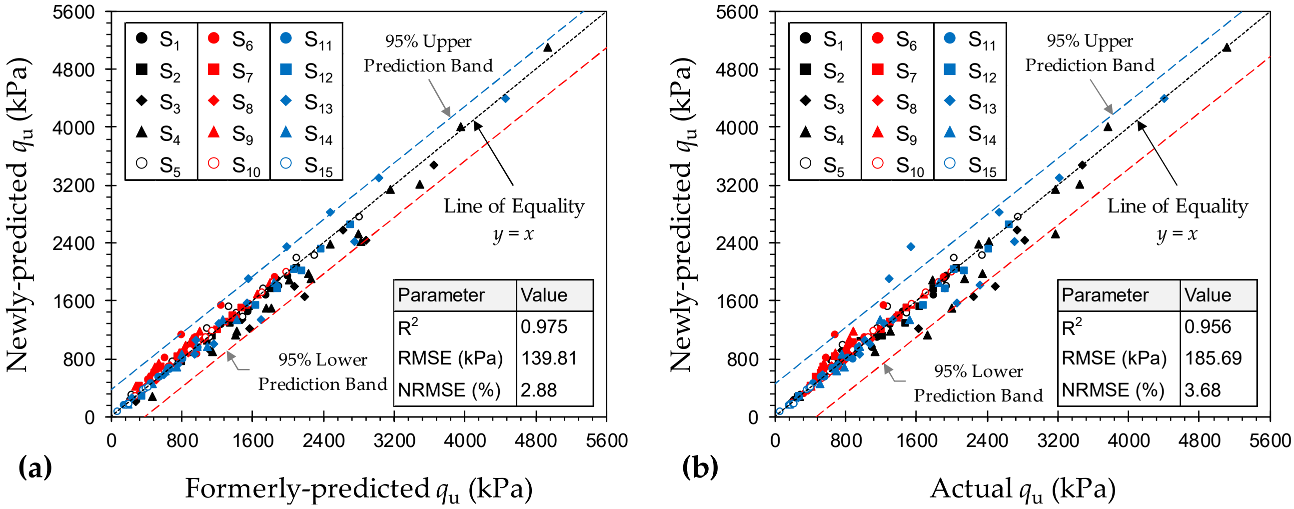

Figure A1. Variations of the reported UCS data against curing time for the fifteen soil–cement datasets (legends represent the binder content): (**a**) S_1; (**b**) S_2; (**c**) S_3; (**d**) S_4; (**e**) S_5; (**f**) S_6; (**g**) S_7; (**h**) S_8; (**i**) S_9; (**j**) S_{10}; (**k**) S_{11}; (**l**) S_{12}; (**m**) S_{13}; (**n**) S_{14}; and (**o**) S_{15}.

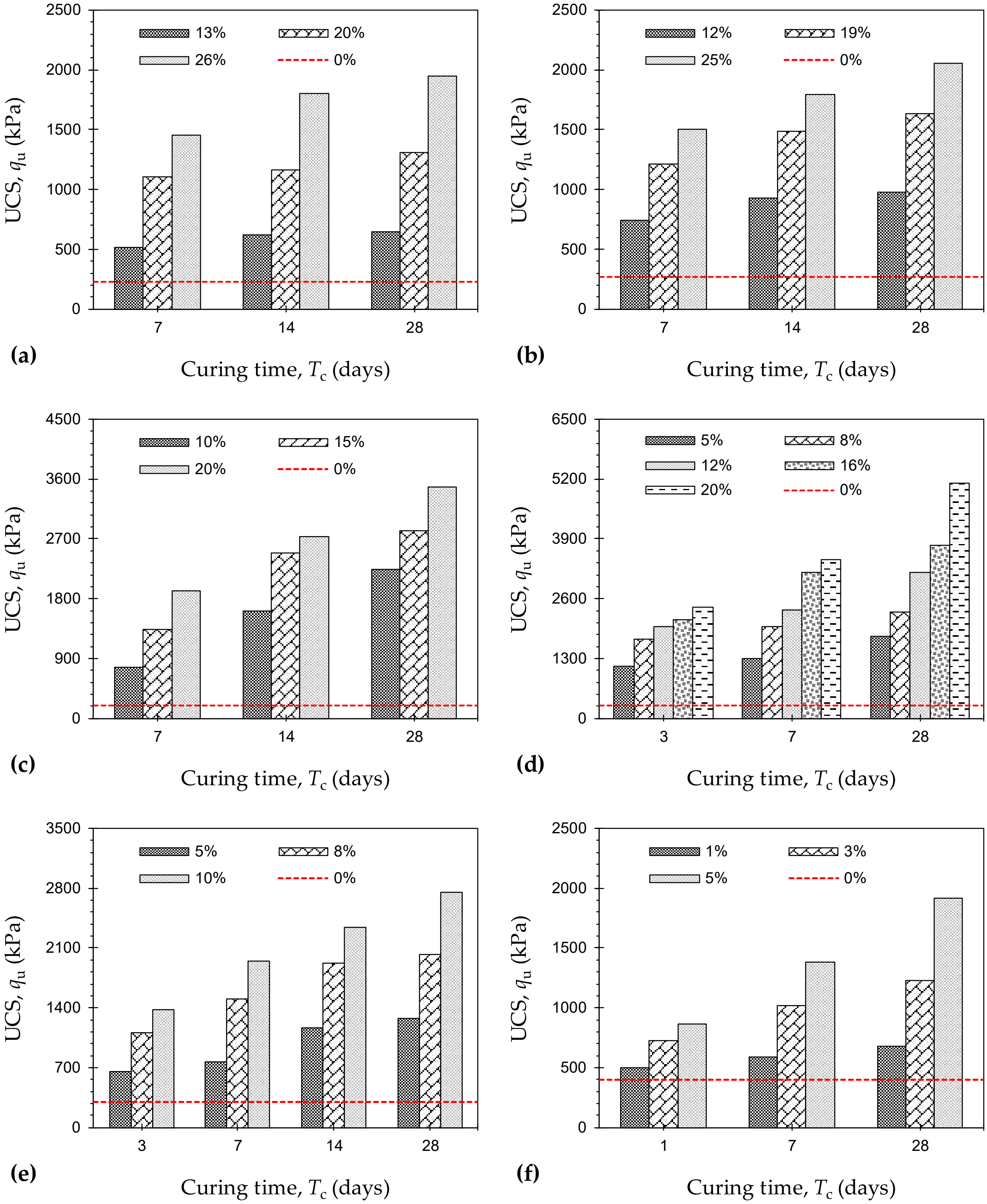

Figure A1. Continued

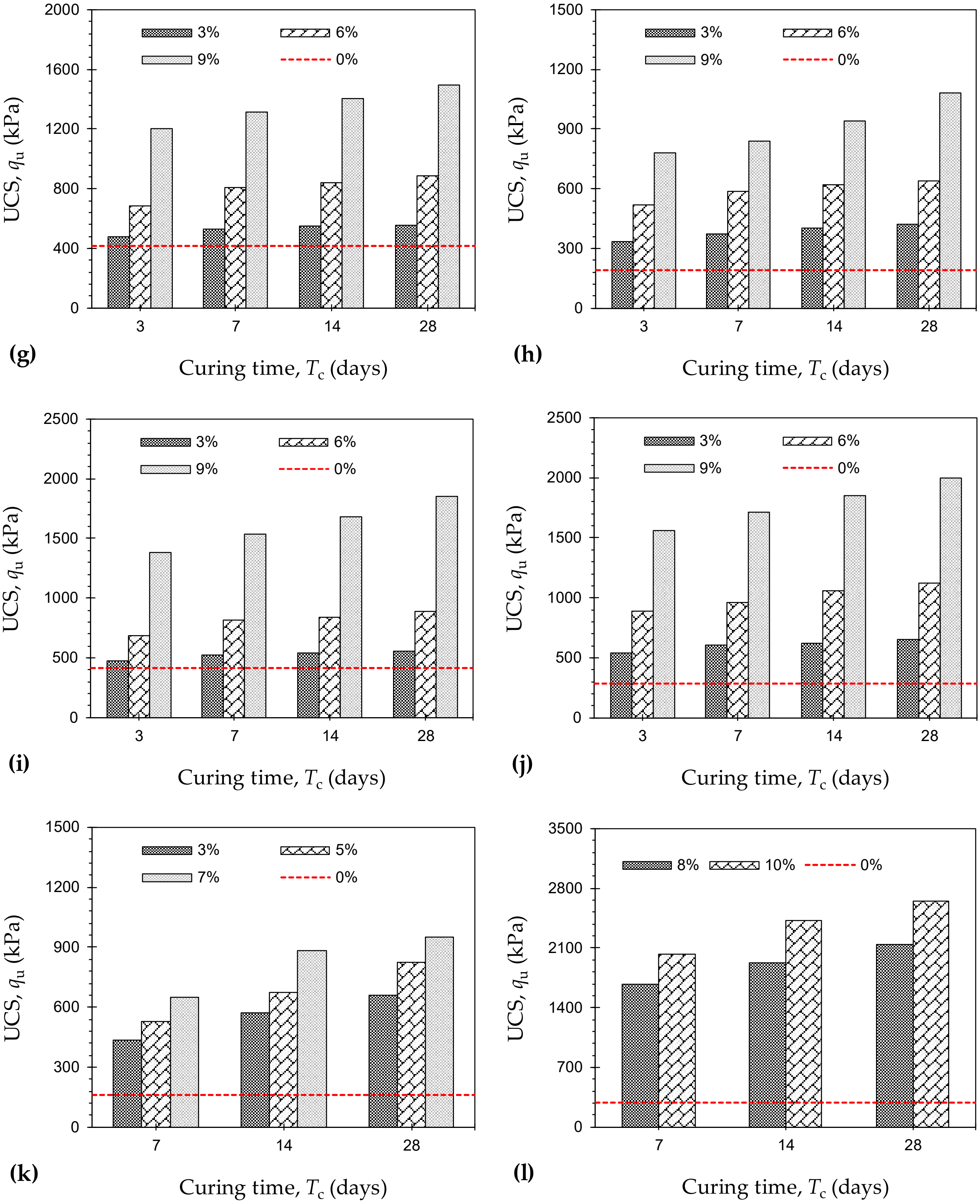

Figure A1. Continued

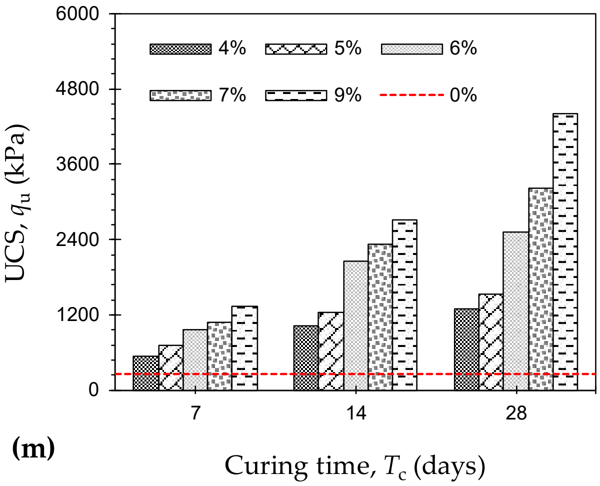
6000
4800
3600
2400
1200
0
UCS, q_u (kPa)
4%
5%
6%
7%
9%
0%
7
14
28
Curing time, T_c (days)

(m)

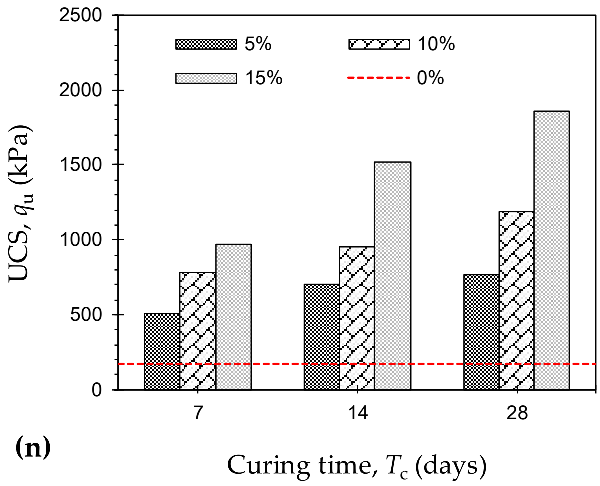
2500
2000
1500
1000
500
0
UCS, q_u (kPa)
5%
10%
15%
0%
7
14
28
Curing time, T_c (days)

(n)

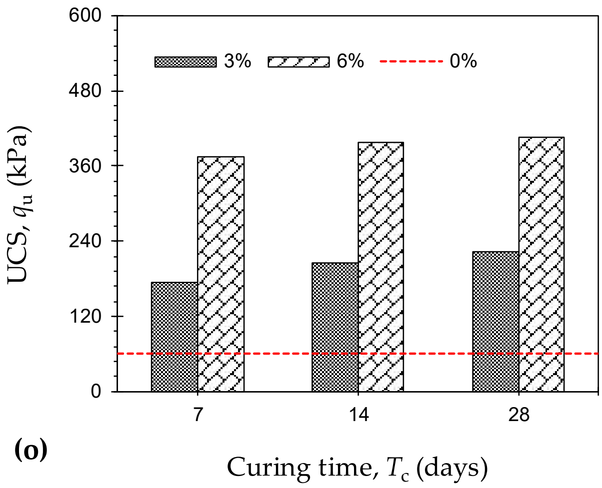
600
480
360
240
120
0
UCS, q_u (kPa)
3%
6%
0%
7
14
28
Curing time, T_c (days)

(o)

List of Tables

Main Text

Appendix A

Table 1. Summary of the regression analysis outputs with respect to the proposed dimensional model or Equation (13).

Dataset	p-value (F)	β_0	$\beta_1 \mid p$-value (T)	$\beta_2^* \mid p$-value (T)	R^2	RMSE (kPa)	NRMSE (%)
S_1	8.22×10^{-7}	1.20×10^{-2}	$-5.43 \mid 5.78 \times 10^{-6}$	$0.179 \mid 3.13 \times 10^{-3}$	0.982	73.14	4.25
S_2	8.61×10^{-7}	6.76×10^{-3}	$-3.28 \mid 3.50 \times 10^{-5}$	$0.223 \mid 2.54 \times 10^{-4}$	0.982	69.40	3.88
S_3	1.67×10^{-5}	1.60×10^{-5}	$-2.05 \mid 4.20 \times 10^{-2}$	$0.479 \mid 1.64 \times 10^{-4}$	0.958	197.75	6.03
S_4	4.45×10^{-10}	8.79×10^{-3}	$-3.73 \mid 7.17 \times 10^{-7}$	$0.250 \mid 1.38 \times 10^{-7}$	0.964	213.31	4.42
S_5	1.36×10^{-9}	1.48×10^{-3}	$-10.99 \mid 4.48 \times 10^{-7}$	$0.283 \mid 1.93 \times 10^{-7}$	0.983	88.05	3.57
S_6	3.69×10^{-6}	2.38×10^{-2}	$-14.88 \mid 1.35 \times 10^{-4}$	$0.194 \mid 5.86 \times 10^{-5}$	0.973	74.21	4.89
S_7	1.06×10^{-10}	2.33×10^{-1}	$-13.68 \mid 4.07 \times 10^{-10}$	$0.094 \mid 1.07 \times 10^{-4}$	0.990	36.47	3.38
S_8	1.06×10^{-11}	6.45×10^{-2}	$-12.24 \mid 1.16 \times 10^{-10}$	$0.130 \mid 6.56 \times 10^{-7}$	0.994	19.95	2.23
S_9	2.36×10^{-9}	9.84×10^{-2}	$-17.08 \mid 1.28 \times 10^{-8}$	$0.118 \mid 7.01 \times 10^{-4}$	0.982	65.84	4.58
S_{10}	3.50×10^{-15}	1.83×10^{-1}	$-15.85 \mid 3.40 \times 10^{-14}$	$0.106 \mid 8.78 \times 10^{-9}$	0.999	19.04	1.11
S_{11}	7.47×10^{-7}	1.44×10^{-3}	$-5.03 \mid 2.68 \times 10^{-3}$	$0.275 \mid 1.95 \times 10^{-5}$	0.982	29.09	3.70
S_{12}	2.05×10^{-5}	2.85×10^{-2}	$-9.02 \mid 9.38 \times 10^{-4}$	$0.194 \mid 6.05 \times 10^{-4}$	0.996	48.24	2.04
S_{13}	4.17×10^{-9}	2.51×10^{-8}	$-10.35 \mid 2.49 \times 10^{-4}$	$0.696 \mid 3.11 \times 10^{-7}$	0.949	241.40	5.83
S_{14}	1.11×10^{-6}	4.99×10^{-5}	$-4.71 \mid 2.26 \times 10^{-4}$	$0.380 \mid 4.84 \times 10^{-5}$	0.980	65.25	3.86
S_{15}	4.49×10^{-5}	6.84×10^{-2}	$-20.09 \mid 1.61 \times 10^{-4}$	$0.096 \mid 2.35 \times 10^{-2}$	0.994	10.00	2.90

Notes:

(F) = Fisher's F-test; and (T) = Student's t-test.

Table 2. Summary of the sensitivity analysis results with respect to the proposed dimensional model or Equation (13).

Plasticity Class	**Datasets**	**Variable, x_a**	$S^{PN}(x_a)$	$S^{P}(x_a)$	$S^{N}(x_a)$	$S^{P\%}(x_a)$ (%)
Low (CL–ML, ML, CL)	S_1, S_3, S_{15}	Binder content, B_c	0.63	0.63	0	54
		Curing time, T_c	0.53	0.53	0	46
Intermediate (MI, CI)	S_2, S_4–S_8, S_{10}	Binder content, B_c	0.86	0.86	0	65
		Curing time, T_c	0.46	0.46	0	35
High (MH, CH)	S_1, S_9, S_{11}, S_{12}, S_{14}	Binder content, B_c	1.13	1.13	0	77
		Curing time, T_c	0.33	0.33	0	23

Notes:

$\dfrac{\partial q_u}{\partial B_c} = \dfrac{\beta_o \sigma_o P_1^{(\beta_1 - 1)} P_2^{\beta_2^*} \left[(\beta_1 + \beta_2^*) P_1 - 2\beta_1 \right]}{1 + B_c}$; and $\dfrac{\partial q_u}{\partial T_c} = \dfrac{\beta_o \beta_2^* \sigma_o P_1^{\beta_1} P_2^{\beta_2^*}}{T_c}$

Table A1. Detailed description of the natural soils' index properties — that is, S_1 to S_{15} without binder.

Soil	S_c (%) [1]	f_c (%) [2]	w_L (%) [3]	I_P (%) [4]	S_a^S (m^2/g) [5]	USCS Classification [6]	Reference
S_1	2	98	55.0	40.0	60.90	CH (Fat Clay)	[37]
S_2	6	94	48.0	33.0	49.01	CI (Lean Clay)	[37]
S_3	48	52	23.0	6.0	7.06	CL–ML (Sandy Silty Clay)	[37]
S_4	8	92	46.0	23.0	34.83	CI (Lean Clay)	[38]
S_5	7	93	49.0	24.0	36.54	CI (Lean Clay)	[39]
S_6	0	100	45.0	19.0	32.14	CI (Lean Clay)	[40]
S_7	23	77	47.5	22.6	28.71	CI (Lean Clay with Sand)	[41]
S_8 [7]	23	77	41.5	21.1	27.06	CI (Lean Clay with Sand)	[41]
S_9	27	65	53.3	27.2	28.51	CH (Sandy Fat Clay)	[42]
S_{10} [8]	27	65	42.4	20.2	22.01	CI (Sandy Lean Clay)	[42]
S_{11}	0	100	58.0	27.0	43.57	MH (Elastic Silt)	[43]
S_{12}	27	65	54.8	27.2	28.51	CH (Sandy Fat Clay)	[44]
S_{13}	26	74	24.0	8.5	12.69	CL (Lean Clay with Sand)	[45]
S_{14}	4	96	83.0	54.0	78.86	CH (Fat Clay)	[46]
S_{15}	8	92	34.2	9.4	16.95	ML (Silt)	[47]

Notes:
[1] Sand (0.075–4.75 mm) content; [2] Fines (< 75 μm) content; [3] Liquid limit; [4] Plasticity index; [5] Specific surface area (obtained as per Equation (9)); [6] Unified Soil Classification System [48]; [7] Soil S_7 contaminated with 9% glycerol; and [8] Soil S_9 contaminated with 3% mono-ethylene glycol (MEG).

Table A2. Detailed description of the compiled soil–cement database — that is, S_1 to S_{15} with binder.

Dataset	Binder	S_a^B (m^2/g) [1]	B_c (%) [2]	S_a^M (m^2/g) [3]	C.E. [4]	w_{opt} (%) [5]	ρ_{dmax} (g/cm^3) [6]	T_c (days) [7]	N^* [8]	Reference
S_1	CKD [9]	0.93	0 13 20 26 = B_c^H	60.90 53.10 48.91 45.31	SP [10]	23.30 25.00 25.64 27.00	1.621 1.510 1.509 1.489	7 = T_c^L 14 28 = T_c^H	10	[37]
S_2	CKD	0.93	0 12 19 25 = B_c^H	49.01 43.24 39.88 36.99	SP	16.00 20.20 21.74 22.00	1.785 1.684 1.663 1.633	7 = T_c^L 14 28 = T_c^H	10	[37]
S_3	CKD	0.93	0 10 15 20 = B_c^H	7.06 6.44 6.14 5.83	SP	14.00 17.06 17.24 17.54	1.897 1.754 1.744 1.725	7 = T_c^L 14 28 = T_c^H	10	[37]
S_4	PC I [11]	0.42	0 5 8 12 16 20 = B_c^H	34.83 33.11 32.08 30.70 29.32 27.95	SP	17.50 18.38 17.80 17.58 17.07 16.87	1.753 1.743 1.753 1.763 1.788 1.821	3 = T_c^L 7 28 = T_c^H	16	[38]
S_5	PC II [12]	0.42	0 5 8 10 = B_c^H	36.54 34.73 33.65 32.92	SP	17.00 17.16 17.33 17.35	1.754 1.805 1.774 1.744	3 = T_c^L 7 14 28 = T_c^H	13	[39]
S_6	OPC [13]	0.51	0 1 3 5 = B_c^H	32.14 31.83 31.19 30.56	SP	21.00 22.60 24.60 25.50	1.690 1.660 1.620 1.600	1 = T_c^L 7 28 = T_c^H	10	[40]
S_7	PC I	0.41	0 3 6 9 = B_c^H	28.71 27.86 27.01 26.16	SP	16.33 18.50 19.50 18.13	1.810 1.772 1.746 1.788	3 = T_c^L 7 14 28 = T_c^H	13	[41]
S_8	PC I	0.41	0 3 6 9 = B_c^H	27.06 26.26 25.46 24.66	SP	15.00 16.10 14.20 13.70	1.846 1.825 1.865 1.832	3 = T_c^L 7 14 28 = T_c^H	13	[41]
S_9	PC I	0.41	0 3 6 9 = B_c^H	28.51 27.66 26.82 25.98	SP	16.30 18.10 18.70 18.10	1.805 1.785 1.744 1.785	3 = T_c^L 7 14 28 = T_c^H	13	[42]
S_{10}	PC I	0.41	0 3 6 9 = B_c^H	22.01 21.36 20.71 20.06	SP	15.60 15.60 17.20 16.40	1.815 1.785 1.795 1.815	3 = T_c^L 7 14 28 = T_c^H	13	[42]
S_{11}	PC II	0.38	0 3 5 7 = B_c^H	43.57 42.28 41.41 40.55	MP [14]	23.70 23.93 24.62 25.29	1.460 1.420 1.400 1.370	7 = T_c^L 14 28 = T_c^H	10	[43]
S_{12}	PC II	0.38	0 8 10 = B_c^H	28.51 26.26 25.69	SP	17.20 16.35 16.00	1.744 1.776 1.785	7 = T_c^L 14 28 = T_c^H	7	[44]
S_{13}	OPC	0.51	0 4 5 6 7 9 = B_c^H	12.69 12.25 12.13 12.00 11.88 11.64	SP	11.50 11.71 11.87 12.12 12.18 12.47	1.710 1.719 1.723 1.735 1.739 1.749	7 = T_c^L 14 28 = T_c^H	16	[45]
S_{14}	OPC	0.51	0 5 10 15 = B_c^H	78.86 74.94 71.02 67.10	SP	18.00 17.30 16.60 16.00	1.713 1.774 1.846 1.927	7 = T_c^L 14 28 = T_c^H	10	[46]
S_{15}	OPC	0.51	0 3 6 = B_c^H	16.95 16.50 16.00	MP	20.89 21.28 21.86	1.690 1.660 1.620	7 = T_c^L 14 28 = T_c^H	7	[47]

Notes:
[1] Specific surface area of the cementitious binder; [2] Binder content (by dry mass of soil); [3] Specific surface area of the soil–binder mixture; [4] Compactive effort; [5] Optimum water content (= w_c^M); [6] Maximum dry density (= ρ_d^M); [7] Curing time; [8] Number of experimental UCS data; [9] Cement kiln dust; [10] Standard Proctor; [11] Portland cement type I; [12] Portland cement type II; [13] Ordinary Portland cement; and [14] Modified Proctor.